JOURNAL OF PROPULSION AND POWER
Vol. 20, No. 4, July–August 2004

Flow Characteristics in a Transonic Ultra-Low-Aspect-Ratio Axial Turbine Vane

Naoki Kuno* and Toyotaka Sonoda†
Honda R&D Co., Saitama 351-0193, Japan

Low-aspect-ratio (low-AR) nozzle guide vanes (NGVs) have rarely been adopted as components of conventional turbines because of poor performance caused primarily by increases in secondary flow losses due to the low AR. However, there are considerable benefits to adopting low-AR NGVs. For example, the number of NGVs is decreased, rotor blade (RB) resonance is eliminated over the order of the count of NGVs from 0% rpm up to the maximum rotational speed. A unique single-stage high-pressure turbine has been developed that is characterized by ultra-low-AR (span height/axial chord = 0.30) NGV that produces no RB resonance. In the development stage, an unusual high-loss region was observed approximately midway between the blades near the hub wall at the NGV exit. The high loss region is described and its causes through are clarified computational fluid dynamics analyses and rig test results, in the context of producing a high-performance turbine component. The main reason for the high loss region was found to be an axial cavity below the hub wall between the NGV and the RB. The fillet of the NGV at the trailing edge on the hub wall also significantly increases the losses.

Nomenclature

k	=	specific heat ratio
P_{loss}	=	$(P_{t4} - P_t)/P_{t4}$
P_s	=	static pressure
P_t	=	total pressure
T_t	=	total temperature
α	=	flow angle
π	=	expansion ratio, P_{t4}/P_{t5}
τ	=	temperature ratio, T_{t4}/T_{t5}

Subscripts

4	=	inlet plane of nozzle guide vane (NGV)
5	=	exit plane of rotor blade (RB), 2.5 axial chord downstream of the trailing edge of RB at mean section
45	=	exit plane of NGV, inlet plane at RB, 10 mm downstream of the trailing edge of NGV

Introduction

TO avoid rotor blade resonance with the nozzle guide vanes (NGVs), it is necessary to decrease the number of NGVs and lower their aspect ratio, maintaining an appropriate solidity to sustain performance. Because of the large secondary flow losses that are generated in the vicinity of the low aspect ratio (span height/axial chord at hub) (AR) vane hub, it is difficult to produce a turbine utilizing low-AR NGVs.

The test results for low-AR NGVs from Williamson et al. demonstrate that secondary flow losses due to low-AR NGVs increased near the hub as compared with other radial locations, though their NGVs seem to not have had sufficiently low AR to avoid resonance.[1] It is necessary to decrease the number of NGVs and make the AR much lower than 1.25 to avoid resonance for their NGV.

Received 5 July 2002; presented as Paper 2002-3644 at the AIAA/ASME/SAE/ASEE 38th Joint Propulsion Conference and Exhibit, Indianapolis, IN, 7–10 July 2002; accepted for publication 19 January 2004.

*Assistant Chief Engineer, Research Laboratory 4, Wako Research Center, 1-4-1 Chuo, Wake City; naoki_kuno@n.w.rd.honda.co.jp.

†Chief Engineer, Research Laboratory 4, Wako Research Center, 1-4-1 Chuo, Wake City; toyotaka_sonoda@n.w.rd.honda.co.jp.

Theoretical predictions by Dunham and Came,[2] Kacker and Okapuu,[3] and Moustapha et al.[4] indicate that secondary flow loss is approximately proportional to the AR of the NGV. According to their predictive model, the AR is assumed to be at least greater than unity. A value below unity is assumed to be out of the range of the predictive models, and there are no test data to verify the prediction models for this (below unity) assumption. Therefore, utilizing their loss model, the secondary flow losses in the case of ultra-low AR for the NGV become significant.

An example of low AR NGVs in manufactured products is the NGV for an annular combustor with centrifugal fuel injection and a lateral supply. A low-AR NGV with a low count was adopted as part of the jet engine for a missile to widen the section area of the blade and ensure sufficient airflow into the combustor. It has, however, not been established whether both lack of resonance and high performance were achieved with this NGV.

With the assumption that the secondary flow loss would not increase significantly, the development of a unique high-pressure turbine (HPT) component consistent with no resonance and high performance was initiated. As predicted at the beginning of the development process, a large loss was observed near the hub of the NGV. Moreover an unusually large loss core, whose location was not explained by conventional theory, was observed at the hub. The loss core was located approximately midway between the blades and near the hub wall. This was independent of the wake at the exit. This loss was so large that it accounted for a significant fraction of the loss at the hub. It was found that it could be decreased by taking measures to reduce all losses at the hub to improve performance, as discussed later in the "Test Results" subsection. The reason for the loss core, however, is still unresolved. This paper describes research by computational fluid dynamics (CFD) analysis and experimental test results investigating a variety of possible reasons for the presence of the loss core. Rig test results and the CFD analyses may be summarized as follows.

First, a single blade passage analysis was performed on the NGV with a large downstream calculation field as a baseline case. An additional analysis with a shortened downstream length was performed to determine the influence of the location of the unified exit static pressure in the circumferential direction for the rotor blade.

Second, a stage analysis was performed to determine the influence of the rotor blade. Williamson et al.[1] and Moustapha et al.[5] showed in their test results that the flowfield at exit of the NGV is strongly influenced by the rotor blade. A flow phenomenon similar to the loss core was not reproduced, although the flowfield was changed.

Third, an NGV with an axial cavity between the nozzle guide vane and the rotor blade was analyzed. The cavity was assumed to be a closed volume without a flow source. Hunter and Manwaring investigated a sealed cavity in front of and behind the rotor blade at the hub in a turbine component.[6] Shabbir et al.[7] and Wellborn and Okiishi[8] also investigated a compressor-associated cavity at the hub. They[7,8] showed that the influence of the cavity on the flowfield was significant. Neither study, however, considered an interaction with a downstream cavity as investigated in this paper.

Finally, this paper also focuses on the influence of a fillet on the NGV trailing edge. A leading-edge NGV fillet is generally preferable. Sauer et al. focused on the beneficial effect of a leading-edge NGV fillet.[9] In our research, an NGV with a fillet was analyzed based on several assumptions. We expected a thicker trailing edge (due to the NGV fillet) to produce stronger shock waves. We also expected a strong interaction between the shock wave from the trailing edge on the suction surface and the wake from the next vane to generate the loss core approximately midway between the vanes at the hub exit. After analysis, our expectations were found to be incorrect. It was found that an NGV weakens the shock wave from the trailing edge on the pressure side and thickens the boundary layer on the end wall.

Test

Apparatus

We adopted a concurrent rig test system for rapid, efficient development of the turbine component. In this system, after a modified design for an airfoil shape is completed, its performance can be determined with one week of rig tests. Therefore, many blade shapes and configurations can be tested in a short time and at low cost. The system consists of three elements. The first element is the design output, which is utilized by manufacturing designers with little delay. The second element is the manufacturing system, which includes the utlization of exclusive five-axis machines for developing the parts for the turbomachinery rig test. The third element is the test, using an exclusive and flexible test facility. Although it is generally accepted that the critical step in the development is manufacturing the test blade, the blade can actually be manufactured in a few days. Aluminum alloy is utilized for the test blade, which reduces the machining time significantly and facilitates procurement of material in advance.

The test facility consists of an air source with a compressor driven by an electric motor, a torque meter, a gearbox and the rig.

Measurement

Total temperature and total pressure at the inlet were measured at five different points in circumferential and radial locations. This was done to reduce the influence of inlet distortion. Total temperature and total pressure at the exit of the rotor blade (RB) were measured using four rakes, equally spaced in the circumferential direction. The rakes were installed with five sensors in the radial direction. These rakes were rotated 90 deg in intervals of 3 deg to form a one-revolution traverse. Therefore, the time-averaged flowfield at each operating point could be measured accurately, including small variations, especially the effect of small variations in tip clearance. Total pressure at the exit of the NGV was traversed and measured across approximately one pitch using five-hole pitot tube.

Flow rate measurement was performed with a vorticity flow meter. Efficiency was calculated from total pressure and total temperature. Torque meter measurements were used as a check and to improve the reliability of the efficiency measurements based on pressure and temperature. A summary of these measurements is shown in Table 1.

When measurement error is considered, the efficiency had an error of $\pm 0.4\%$. The error in the pressure measurement was $\pm 0.1\%$. The error in the temperature measurement was ± 0.5 K. The error in the efficiency does not include the effect of heat transfer. The heat transfer of the probe and the casing in the rig was assumed to be very small because heat insulation material was wrapped around the sensors and the turbine exit temperature was adjusted to be as close as possible to the test room temperature.

Table 1 Measurement locations

Parameter	Method	Location and number of measurement: Circumferential	Radial	Total
Inlet of NGV				
T_{t4}	Fixed	5	5	5
P_{t4}	Fixed	5	5	5
P_{S4}	Static tap	1	2	2
Exit of NGV[a]				
P_{t45}	Traverse	1	7	161
α_{45}	Traverse	1	7	161
Exit of RB				
T_{t5}	Traverse	4	5	600
P_{t5}	Traverse	4	5	600
P_{S5}	Static tap	1	2	2

[a]Inlet of RB.

Rig

The rig was the same size and scale as the planned engine. The rig layout for stage performance tests is shown in Fig. 1a. The ducts are constructed mainly of stainless steel, and the influence of the combustor return shape is considered in a manner similar to that of the rig used by Woinowsky-Krieger et al.[10] The NGV and RB are fabricated from aluminum. The RB is integrated with the disk manufactured by the five-axis machine. The NGV consists of two parts, the tip shroud and the blade, which is integrated with the hub wall. The blade is connected to the tip shroud by a connecting pin. Thus, the hub side has a fillet, whereas the tip side does not. There is no cooling in the rig, although in an engine, a cooling slit is present in the center of the trailing edge of the NGV. The thickness of the trailing edge of the NGV is set at 1.8 mm, when cooling air ejection from the trailing edge is considered. There is no cooling for the RB in either the rig or engine, and so the thickness of the trailing edge is set to 0.5 mm. Specifications for the design are shown in Table 2. Velocity triangles at midspan are shown in Fig. 1b. This specification is conventional except for the low-AR NGV and RB with minishroud, which has a similar fillet at the tip.

Test Results

To attain higher efficiency in the final blade design, many different approaches were tested. With regard to the NGV, the optimum lean angle and a shorter axial distance between the NGV and RB were considered and adopted. With regard to the RB, adding a minishroud on the tip and hub contouring were considered and adopted (not shown here).

The efficiency of the final blade shape in the rig test was 87.9%, near the design point. This efficiency was evaluated from P_{t4}, T_{t4}, P_{t5}, and T_{t5}. The efficiency (adiabatic efficiency $= [1-(1/\tau)]/[1-(1/\pi)^{(k-1)/k}]$), expansion ratio, temperature ratio, and exit flow angle of the circumferential averaged distribution in span height are shown in Figs. 2, 3, 4, and 5, respectively. The stage analysis results from CFD, which was used as an analysis tool in this paper, predicted an efficiency of 88.4%, are also shown in Figs. 2–5. FINE/Turbo was utilized as the CFD code. Experimental results and the CFD analysis are in agreement except for the flow field near the tip shroud. The difference in efficiency is mainly due to the difference in temperature ratio. CFD overestimated the temperature ratio near the tip shroud. The adoption of a rotor with a minishroud might be one reason for the difference. CFD could not possibly predict the flowfield near the tip clearance with a high degree of accuracy because of the complicated shape and the skewed mesh.

P_{loss} contour test results at the NGV exit with rotor rotating are shown in Fig. 6. Traverse measurements were performed along one pitch at the locations marked by the intersections of the dotted lines shown in Fig. 6. Data from two pitches were doubled for illustrative purposes in Fig. 6. The blank at the endwall indicates the end of the

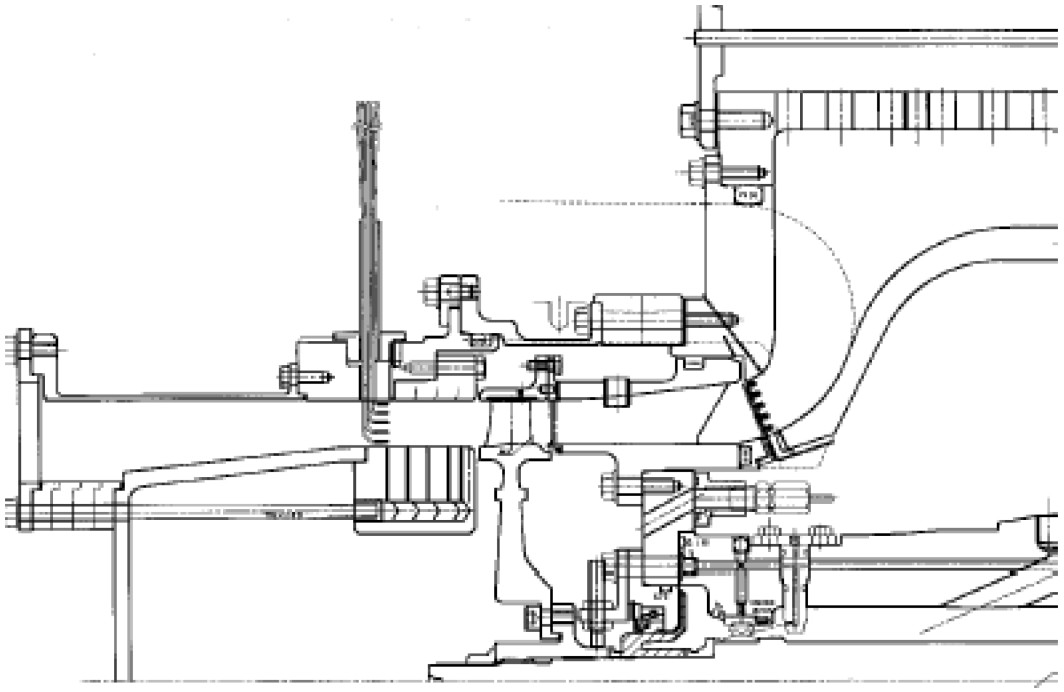

Fig. 1a Rig layout (at stage performance test).

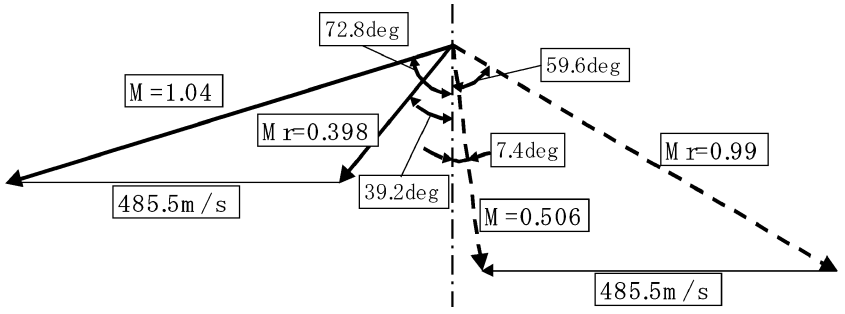

Fig. 1b Velocity triangles at midspan.

Table 2 Design specifications

Parameter	Value
Corrected mass flow rate	0.87 kg/s
Expansion ratio	3.04
NGV counts	8
RB counts	51
NGV AR	0.3
TE thickness of NGV at span height	1.8 mm
Exit span height of NGV	18.9 mm
Rotational tip speed of RB	525 m/s
Loading factor	1.375
Flow coefficient	0.531
Reaction based on enthalpy	0.324

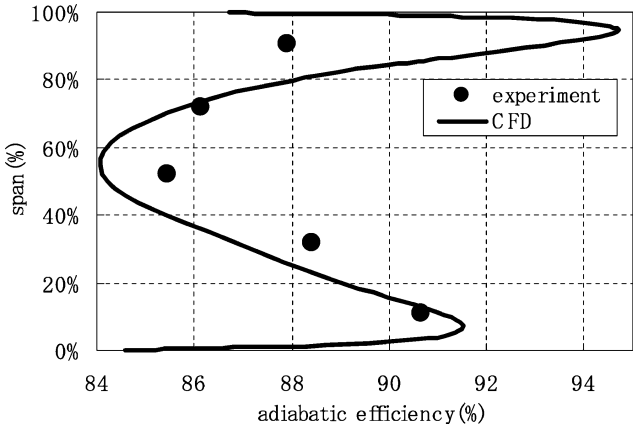

Fig. 2 Adiabatic efficiency.

measurement range. The wakes are inclined because the NGV was inclined. Two loss cores are observed. One is viewed as conventional; it develops from the passage vortex and combines with the wake on the suction side. The other is viewed as an unconventional loss core; the reasons for its appearance are unclear. It is indicated by the ellipse in Fig. 6. It is located approximately midway between the NGV at the hub.

Computational Model

NGV Calculation (Baseline Case 1)

The mesh size is $49 \times 49 \times 145$ (pitch $\times$ span $\times$ flow direction). An I mesh topology is used, as shown in Fig. 7. The inlet boundary was located at a plane approximately one chord upstream of the leading edge of the NGV. The exit boundary was located at a plane approximately one chord downstream of the trailing edge of the NGV. Static pressure at the boundary exit of the calculation was fixed on the hub, and we assumed radial equilibrium. The Baldwin–Lomax turbulence model was used. An alternative is the k–ε turbulence model, but in the case of a skew mesh, as in the analysis with the axial cavity and fillet, the k–ε model tends to overgenerate

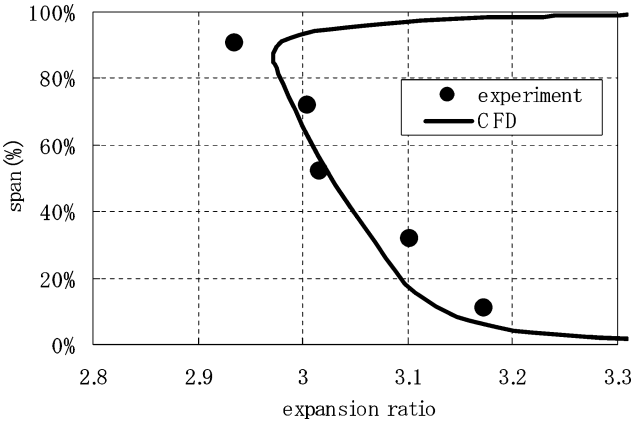

Fig. 3 Expansion ratio.

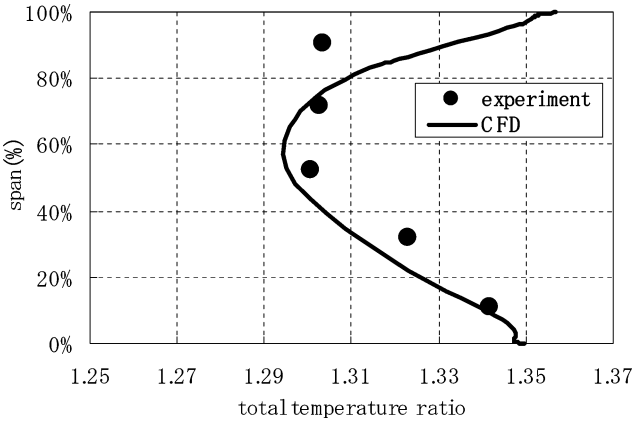

Fig. 4 Temperature ratio.

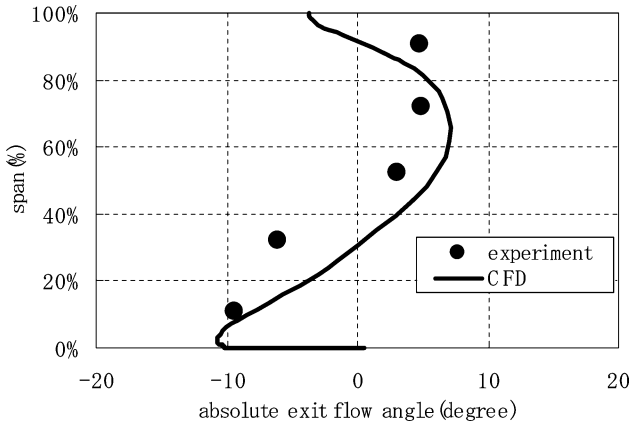

Fig. 5 Absolute exit flow angle.

the turbulent viscosity more than the Baldwin–Lomax model does. The Baldwin–Lomax model was therefore, adopted to provide the same conditions in all of the analyses. This analysis is a baseline for the following analyses.

NGV Calculation with Short Downstream Length (Case 2)

The mesh size is 49 × 49 × 129 (pitch × span × flow direction). An I mesh topology is used, as shown in Fig. 8. The other conditions are the same as case 1. The exit boundary on the hub was located on the plane 10 mm downstream of the trailing edge, simulating the location of RB.

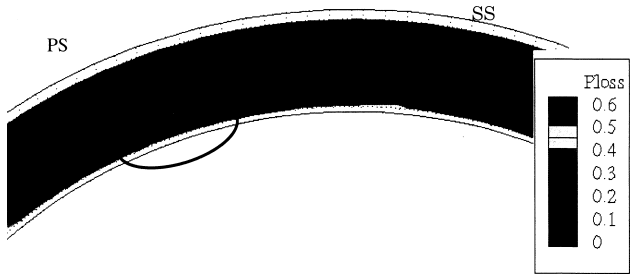

Fig. 6 P_{loss45} contours at NGV exit (test results).

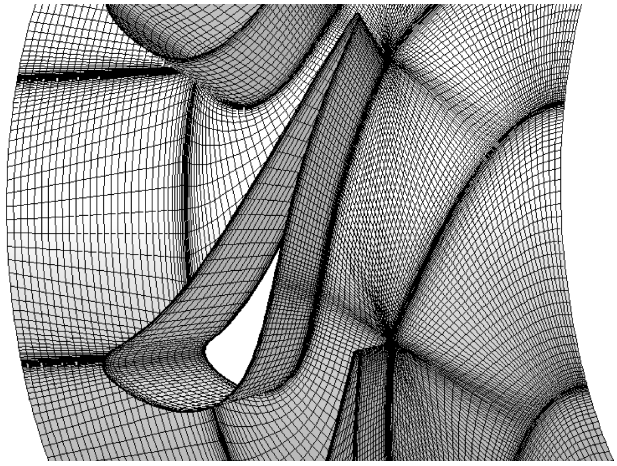

Fig. 7 Computational mesh (baseline).

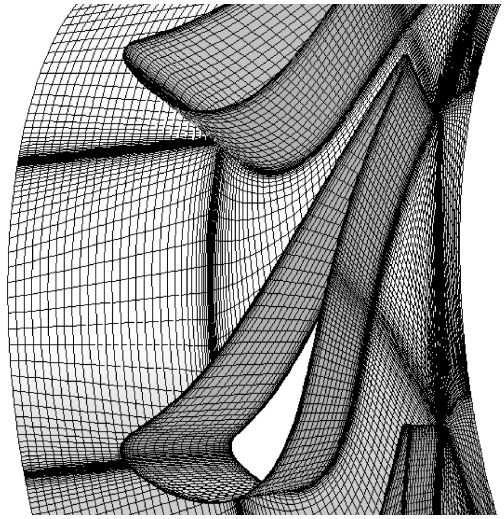

Fig. 8 Computational mesh (short downstream length).

Steady-State Stage Calculation (Case 3)

A mixing plane was utilized between the NGV and RB. All of the physical quantities at the mixing plane were averaged in the circumferential direction. The mesh size of the NGV is 49 × 49 × 129 (pitch × span × flow direction). The mesh size of the RB is 49 × 49 × 129 (pitch × span × flow direction). Both grids use an I mesh topology, as shown in Fig. 9. Static pressure at the exit of the RB was fixed at the hub. The value was adjusted to achieve the total expansion ratio in the rig test. The other conditions were the same as case 1.

NGV Calculation with Cavity (Case 4)

The mesh size for the NGV is 49 × 49 × 144 (pitch × span × flow direction). An H mesh topology is used, as shown in Fig. 10. This is required because it must coincide with the mesh of the

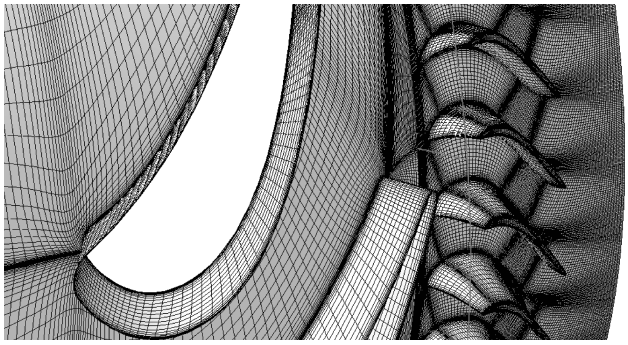

Fig. 9 Computational mesh (steady-state stage).

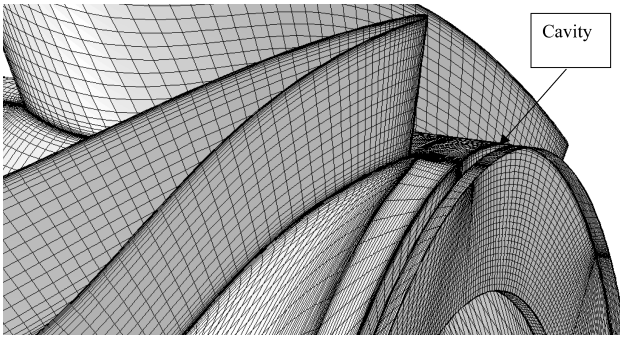

Fig. 10 Computational mesh with axial cavity.

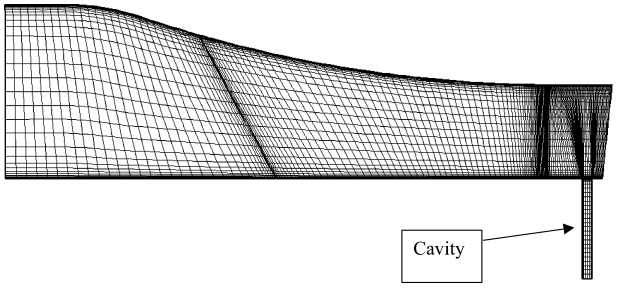

Fig. 11 Meridional view of computational mesh with axial cavity.

cavity at the boundary due to the structural grid having to admit a section of skew mesh. The meridional mesh is shown in Fig. 11. The cavity was located 8 mm downstream of the trailing edge of the NGV. The axial width was 2 mm. The depth was assumed to be 18.6 mm, which is equivalent to the NGV span height. In the experimental rig, the cavity is connected to one large volume, as shown in Fig. 1a. In the calculation, a depth of 18.6 mm was judged to be sufficient to simulate the influence of the axial cavity qualitatively. It was assumed that the main flow from the cavity was not sealed, as in the rig test, which was a closed volume, although an air seal was supplied in the engine. The mesh size of cavity was $9 \times 49 \times 33$ (axial $\times$ circumferential $\times$ depth direction).

High AR NGV Calculation with Cavity (Case 5)

To determine the influence of AR, the NGV was scaled by half in both the axial and circumferential directions, and double the NGV count was analyzed without changing the span height. Calculation boundaries were also scaled. The other conditions were the same as in case 4. The mesh is shown in Fig. 12.

NGV Calculation with Fillet (Case 6)

The radius of the fillet was 2 mm. Only the hub side has the fillet in the rig. There is no fillet on the tip side in the rig, as described before, due to the assembly structure. The other conditions were the same as in case 1. The mesh size of the NGV is $49 \times 49 \times 147$ (pitch $\times$ span $\times$ flow direction). An H mesh topology is used, as shown in Fig. 13.

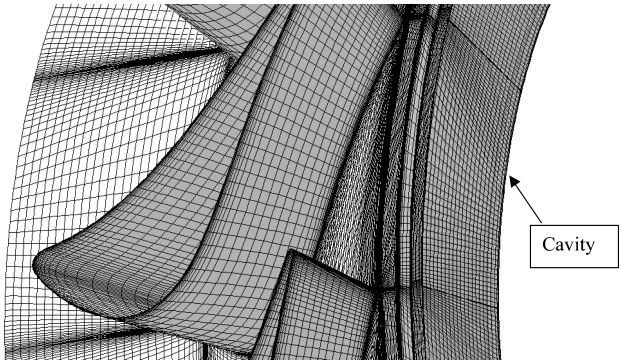

Fig. 12 Computational mesh of high-AR NGV with axial cavity.

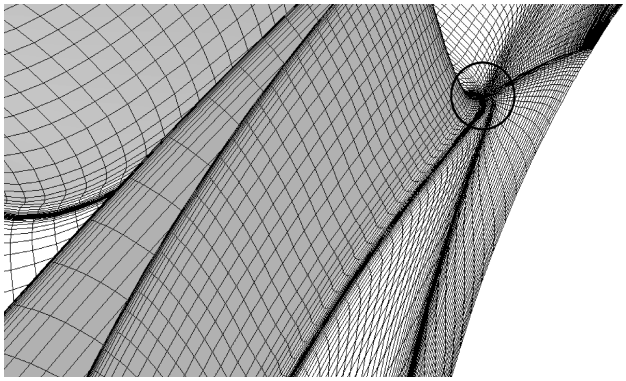

Fig. 13 Computational mesh with fillet at hub.

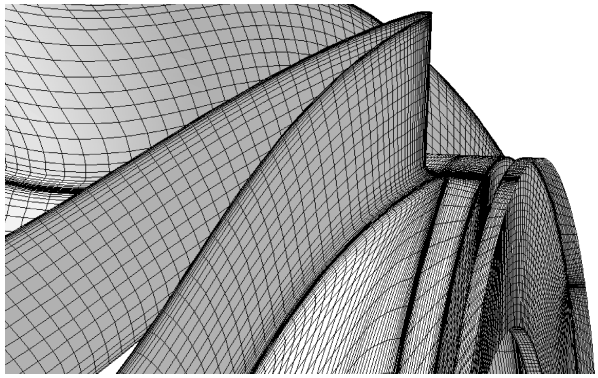

Fig. 14 Computational mesh with axial cavity and fillet at hub side.

The influence of the fillet was considered to be modeled only qualitatively because the mesh in the vicinity of the fillet was skewed. The vicinity of the fillet on the trailing edge is shown marked with a circle in Fig. 13.

NGV Calculation with Axial Cavity and Fillet (Case 7)

Based on the results of analyses of cases 4 and 6, an analysis of the NGV with both the axial cavity and fillet was performed. It was not possible to generate a mesh to provide high-quality coverage of both the cavity and fillet, but this analysis was considered sufficient for a preliminary consideration of the phenomenon. An H mesh topology was used, as shown in Fig. 14.

Discussion of Results

NGV Calculation (Baseline Case 1)

The loss core between the NGVs at the exit was not reproduced by this CFD analysis, which was similar to the one obtained in a previous design process (not shown here) with a different commercial

Fig. 15 P_{loss45} contours at NGV (baseline).

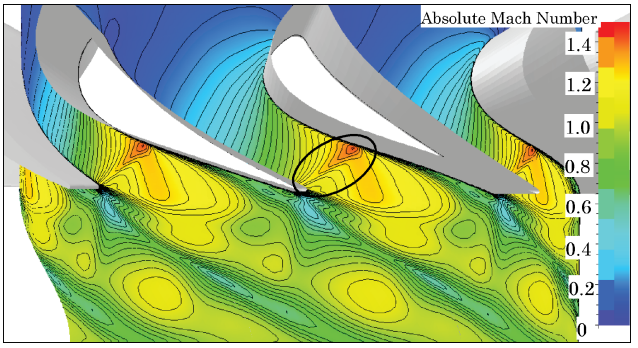

Fig. 16 Mach number contours near hub section (baseline).

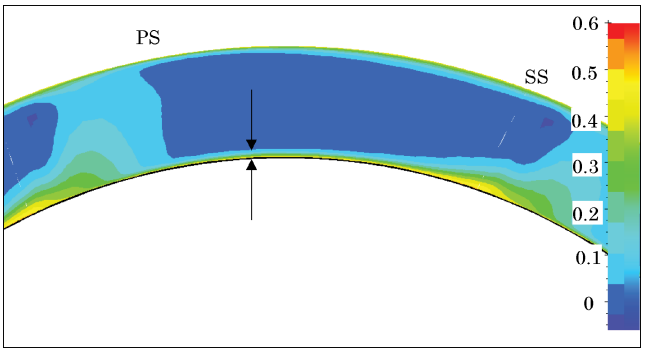

Fig. 17 P_{loss45} contours at NGV exit in short downstream length.

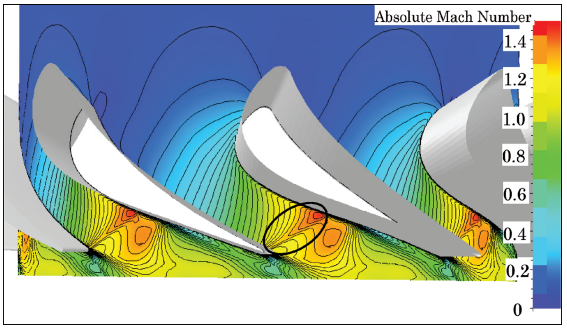

Fig. 18 Mach number contours near hub section in short downstream length.

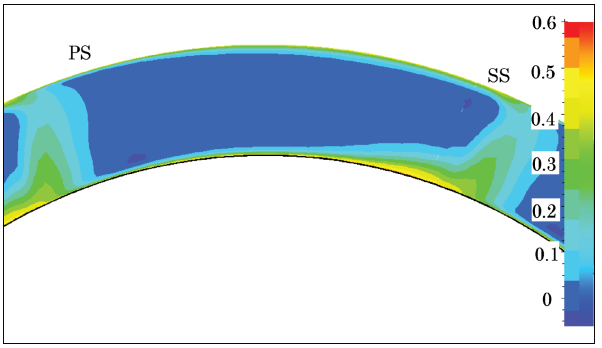

Fig. 19 P_{loss} contours at NGV exit (stage analysis).

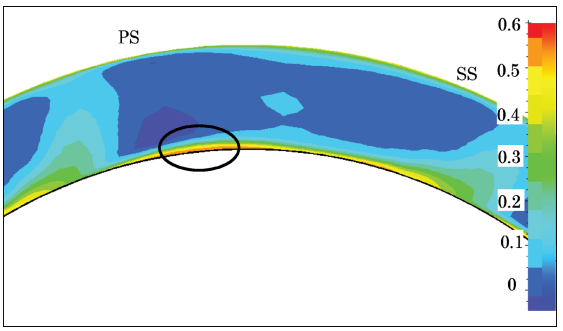

Fig. 20 P_{loss45} contours at NGV exit with cavity.

CFD code. P_{loss45} contours are shown in Fig. 15. Figure 15 shows a wake at the trailing edge, a fully developed thick boundary layer at the endwall, and a conventional loss core, which was generated from the passage vortex and adhered to a wake.

Mach number contours at 3.3% span height from the hub are shown in Fig. 16. We observed that a shock wave was generated at the trailing edge on the pressure side with a reflection on the suction surface. The boundary layer on the suction surface separated from the region on the suction surface and transformed into the wake.

NGV Calculation with Short Downstream Length (Case 2)

P_{loss45} contours are shown in Fig. 17. The contours are similar to the case 1 baseline (Fig. 15), and the loss core was not reproduced by this CFD analysis, either. The contours were similar because the same static pressure at the exit boundary was forced to be uniform in the circumferential direction, although the location was different. The wake is wider in this analysis than in case 1 baseline. The reason for this is that the mixing at the short exit boundary is promoted more than at the long exit boundary in case 1 baseline.

Mach number contours at 3.3% span height from the hub are shown in Fig. 18. Unlike the case 1 baseline (Fig. 16), the shock wave is not reflected off the suction surface. It is appropriate to describe another shock wave rather than a reflected shock wave. In short, two shock waves were generated on the suction surface due to the short downstream length.

Steady-State Stage Calculation (Case 3)

P_{loss} contours 4 mm downstream of the trailing edge of the NGV are shown in Fig. 19. This location was adopted as an evaluation plane because the P_{loss45} contour should be averaged in the circumferential direction within the rotor blade calculation field. Figure 19 was found to be similar to the case 1 baseline and the case 2 short downstream Figs. 15 and 17. The loss core was not reproduced by this analysis, either.

NGV Calculation with Cavity (Case 4)

A region similar to the unconventional loss core was observed as shown in Fig. 20. This region is marked with an ellipse in the Fig. 20. Investigating in more detail, we found the following. The static pressure above the cavity varies in the circumferential direction. The difference in static pressure above the cavity leads to the flow in the radial direction. A part of the main flow enters the cavity, and the flow from the cavity exits to the main flow as shown with arrows in Fig. 21. As a result, the flow from the cavity generates the loss core. In an engine, due to the presence of an air seal from the cavity, there is no flow into the cavity. Though the loss core observed in this rig probably does not exist in the engine, we assume that a similar loss core pattern should exist in the engine, with the radial flow over

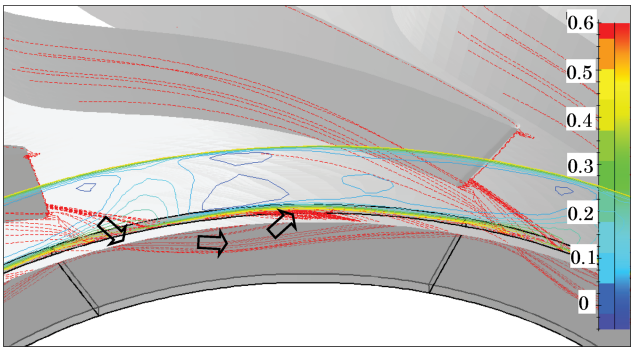

Fig. 21 P_{loss45} contours and stream lines at NGV.

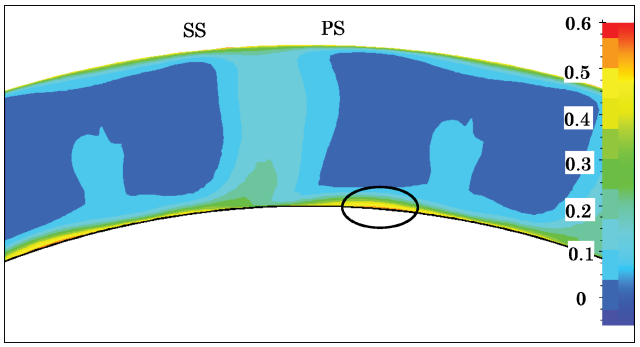

Fig. 22 P_{loss} contours at high-AR NGV exit with cavity.

the cavity. In the case of the presence of the air seal, assessing the changes in the phenomenon experimentally and analytically should be addressed in the future.

There are two unexplainable phenomena in Fig. 20. One is that a loss was generated on the tip shroud between the blades. The other is that a loss was generated at midspan height between blades. The former phenomenon also turned up in the rig test (Fig. 6). These issues will also be investigated in the future.

High AR NGV Calculation with Cavity (Case 5)

A high-AR NGV with a cavity was studied to determine whether the unconventional loss core was also generated in the case of a conventional AR NGV, and in fact, it was, as shown in Fig. 22. It is marked with an ellipse. Regardless of AR, it was found that the same phenomenon arises, a loss core over the cavity. The two unexplainable phenomena present in Fig. 20, also appear in Fig. 22.

P_{loss} distributions in the radial direction averaged in the circumferential direction are shown in Fig. 23. The four curves show the analysis of the low-AR NGV with and without the cavity and the high AR NGV with and without the cavity. Focusing on the differences between the losses near the hub as influenced by the magnitude of AR and the presence of the cavity, we found that the lower the AR was, the larger the influence of the cavity with respect to the loss near the hub. We also found that the loss in main flow with the cavity increases as compared to losses without the cavity. Though the reason for this is not clear, this tendency agrees with the presence of the tip shroud and midspan losses shown in Figs. 20 and 22.

NGV Calculation with Fillet (Case 6)

As shown in Fig. 24, the loss core was not reproduced in the calculation of the NGV with the fillet, either. It was found, however, that the boundary layer on the hub at the exit was larger than the one for the NGV without the fillet (Fig. 17). The boundary layer at the tip side did not change. The reason for this is that the tip section did not have a fillet, to simulate the rig as described earlier.

The phenomena in Figs. 17 and 24 can be explained as follows and as shown in Fig. 25. The passage area increases locally from the throat to the trailing edge on the pressure surface. The flow suddenly decelerates downstream of the throat due to the sudden lack of thickness of the trailing edge. As a result, the boundary layers

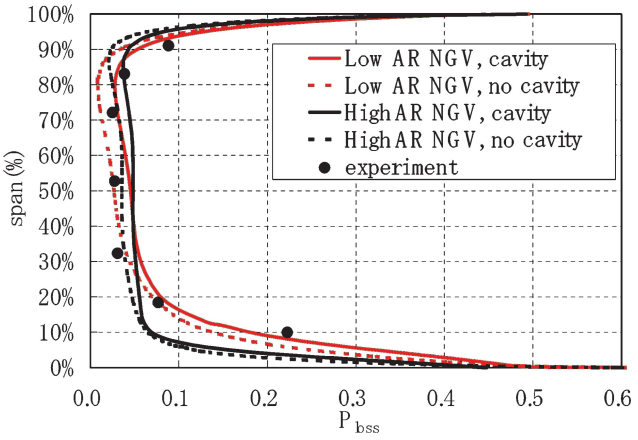

Fig. 23 P_{loss} radial distributions averaged in circumferential direction.

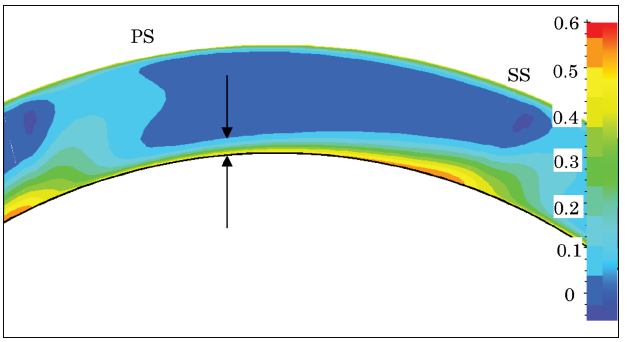

Fig. 24 P_{loss45} contours at NGV exit with fillet.

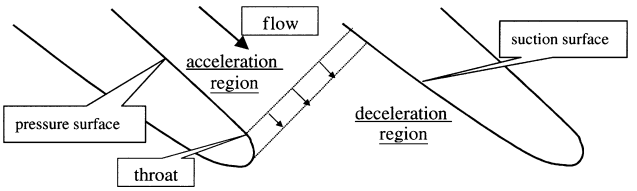

Fig. 25 Schematic diagram of area adjacent to the TE.

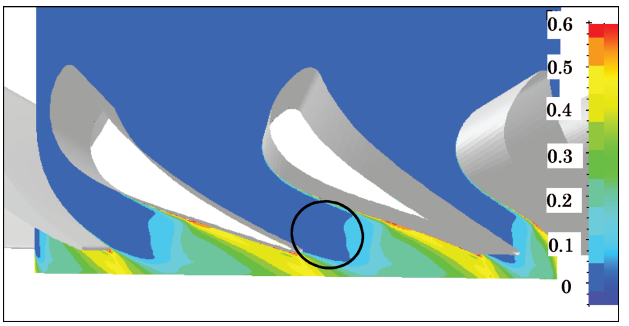

Fig. 26 P_{loss} contours near hub with no fillet.

on the suction surface and on the endwalls develop downstream of the throat. The deceleration of the flow at midspan height, however, tends to be canceled out in the radial direction. The deceleration of the flow on the endwalls tends to increase more, suffering from cancellation at the midspan height. Because of the influence of the fillet, the deceleration at the endwalls is so large that the boundary layers on the suction surface and on the endwalls tend to be much thicker downstream of the throat in the streamwise direction. Consequently, the loss at the endwall of the NGV with the fillet is larger than the case without the fillet in the downstream region around the throat. To support this explanation, P_{loss} contours at 3.3% span height from the hub without the fillet and with the fillet are shown in Figs. 26 and 27. We found that P_{loss} with the fillet increased as

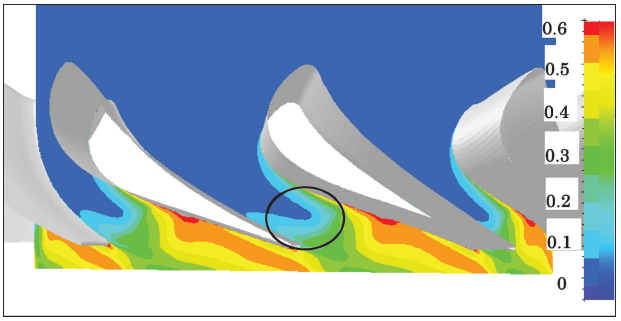

Fig. 27 P_{loss} contours near hub with fillet.

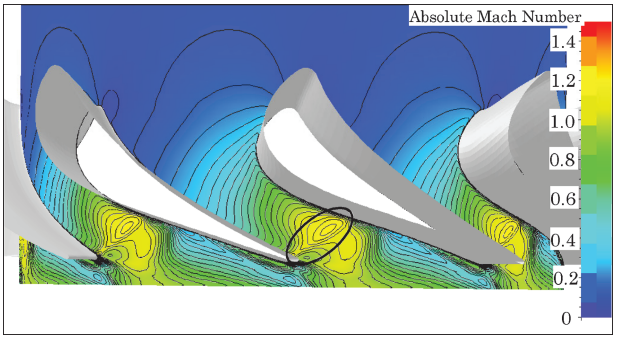

Fig. 28 Mach number contours near hub with fillet.

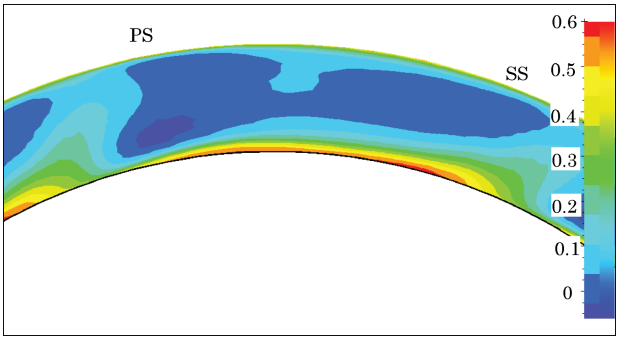

Fig. 29 P_{loss45} contours at NGV exit with cavity and fillet.

compared with the case without the fillet adjacent to the throat and on the suction surface downstream of the throat.

Mach number contours at 3.3% span height from the hub are shown in Fig. 28. The shock wave from the trailing edge toward the suction surface of the NGV with the fillet was weaker than for the one without the fillet (Fig. 18). This phenomenon was the reverse of the speculation that a thicker trailing edge due to the fillet results in stronger shock waves. The reason for this is as follows: P_{loss} with the fillet increased more than for the case without the fillet downstream of the throat in the streamwise direction, as shown in Figs. 26 and 27. The decrease of total pressure adjacent to the throat decelerated the velocity locally, and the shock wave became weaker.

In summary, the losses due to the development of the boundary layer on the suction surface are influenced to a greater extent by the deceleration of the fluid induced by the presence of the fillet at the trailing edge (TE) than by the shock wave to the extent observed in this case.

There is an unexplained phenomenon shown in Fig. 27; a loss was generated on both the suction and pressure surfaces upstream of the throat. This should also be investigated in the future.

NGV Calculation with Axial Cavity and Fillet (Case 7)

An analysis of the NGV with both axial cavity and fillet was performed based on the results of case 4 with cavity and case 6 with fillet. P_{loss} contours are shown in Fig. 29. The boundary layer and the loss core were overestimated as compared with test results, although the phenomena were captured well qualitatively.

Conclusions

In the process of developing an HPT component with no resonance and high performance, an unconventional loss core was observed approximately midway between the blades near the hub wall at the NGV. The cause of this loss core was determined from test results, and a new and unique approach to CFD analysis as follows.

1) A part of the flow from the axial cavity between the NGV and the RB influences the downstream flowfield at the NGV exit, and this generates a loss core independent of the wake.

2) The magnitude of the loss core depends on the AR of the NGV. The lower the AR, the larger is the loss core. Especially in the case of the NGV with AR less than one, the loss becomes significant near the hub.

3) A fillet at the trailing edge of the NGV increases the loss core significantly.

Our research did not consider the influence of the air seal from the cavity. It is important for future work to determine the changes in the loss core in engines, both experimentally and analytically.

Acknowledgments

The authors wish to thank the personnel in the design, manufacturing, and test groups at Honda Research and Development (R&D). We also wish to thank all our colleagues in Research Laboratory 1 at Honda R&D for giving us the opportunity to research this phenomenon.

References

[1]Williamson, R. G., Moustapha, S. H., and Huot, J. P., "The Effect of a Downstream Rotor on the Measured Performance of a Transonic Turbine Nozzle," *Journal of Engineering for Power*, Vol. 108, No. 2, 1986, pp. 269–274.

[2]Dunham, J., and Came, P. M., "Improvements to the Ainley-Mathieson Method of Turbine Performance," *Journal of Engineering for Power*, Vol. 92, No. 2, 1970, pp. 252–256.

[3]Kacker, S. C., and Okapuu, U., "A Mean Line Prediction Method for Axial Turbine Efficiency," *Journal of Engineering for Power*, Vol. 104, No. 1, 1982, pp. 111–199.

[4]Moustapha, S. H., Kacker, S. C., and Tremblay, B., "An Improved Incidence Losses Prediction Method for Turbine Airfoils," *Journal of Turbomachinery*, Vol. 112, No. 2, 1990, pp. 267–276.

[5]Moustapha, S. H., Carscallen, W. E., and McGeachy, J. D., "Aerodynamic Performance of a Transonic Low Aspect Ratio Turbine Nozzle," *Journal of Turbomachinery*, Vol. 115, No. 3, 1993, pp. 400–408.

[6]Hunter, S., and Manwaring, S., "Endwall Cavity Flow Effects on Gas Path Aerodynamics in an Axial Flow Turbine: Part I–Experimental and Numerical Investigation," American Society of Mechanical Engineers, ASME Paper 00-GT-651, May 2000.

[7]Shabbir, A., Celestina, M., Adamczyk, J., and Strazisar, A., "The Effect of Hub Leakage Flow on Two High Speed Axial Flow Compressor Rotors," American Society of Mechanical Engineers, ASME Paper 97-GT-346, June 1997.

[8]Wellborn, S., and Okiishi, T., "The Influence of Shrouded Stator Cavity Flows on Multistage Compressor Performance," *Journal of Turbomachinery*, Vol. 121, No. 3, 1999, pp. 486–498.

[9]Sauer, H., Muller, R., and Vogeler, K., "Reduction of Secondary Flow Losses in Turbine Cascades by Leading Edge Modifications at the Endwall," *Journal of Turbomachinery*, Vol. 123, No. 2, 2001, pp. 207–213.

[10]Woinowsky-Krieger, M., Lavoie, J.-P., Vlasic, E. P., and Moustapha, S. H., "Off-Design Performance of a Single Stage Transonic Turbine," *Journal of Turbomachinery*, Vol. 121, No. 2, 1999, pp. 177–183.